Surface Science 425 (1999) 1–14

Non-adiabatic charge transfer process of oxygen on metal surfaces

Gil Katz [a,]*, Yehuda Zeiri [b], Ronnie Kosloff [a]

[a] *Department of Physical Chemistry and the Fritz Haber Research Center, The Hebrew University, Jerusalem 91904, Israel*
[b] *Department of Chemistry Nuclear Research Center–Negev, PO Box 9001, Beer-Sheva 84190, Israel*

Received 7 August 1998; accepted for publication 10 November 1998

Abstract

The dynamics of charge transfer processes of oxygen on metal surfaces are investigated. The analysis is based on a set of diabatic potential energy surfaces, each representing a different charged oxygen species. Empirical universal potential energy functions have been constructed that mimic the oxygen–silver, oxygen–aluminum and oxygen–cesium systems. The differences between the work functions of these metals are reflected in the potential parameters. The dynamics are followed by solving the multichannel time-dependent Schrödinger equation starting from oxygen in the gas phase. Only the direct short time part of the dynamics is followed leading to the creation O_2^- in the gas phase as well as dissociative chemisorption. A large portion of the wave function is trapped in molecular chemisorption charged states. It is found that the position of the crossing seam between potentials has a profound influence on the outcome.

Keywords: Charge-transfer; Curve-crossing; Metallic surfaces; Oxygen

1. Introduction

A molecule colliding with a metal surface can scatter directly back into the gas phase or become trapped in a potential well. In addition, the molecule can dissociate either directly or by passing through an intermediate trapped state. This dissociation is a key event in heterogeneous catalysis. Attractive dispersion forces universally create a weak potential well where a trapped molecule is only slightly perturbed from its gas-phase structure. In addition, chemisorption states can occur in which strong interactions with the metal are created which alter the molecular structure. Typically, in these states there is a charge transfer from the metal to the molecule. The transition from the physisorption state to the chemisorption state requires, therefore, a change in the electronic structure of the molecule–metal entity. When a neutral molecule interacts with the surface and charged species appear on the surface, and in the gas phase, necessarily non-adiabatic transitions have occurred.

Ion formation via non-adiabatic curve crossing is a well known phenomenon in gases. An electron tunneling from the metal valence band to the affinity level of the molecule is the gas surface analogue. The excess electron can occupy an anti-bonding molecular orbital and lead to dissociation. The metals' work functions and the molecules' electron affinities must, therefore, play a key role in such reactions. A harpooning mechanism has been suggested for the dissociative adsorption of

---

* Corresponding author. Fax: +972-2-6513242;
e-mail: gkatz@fh.husi.ac.il.

PII: S0039-6028(98)00909-1

halogens on alkaline earth metals [1–3]. These ideas have been also generalized to the interaction of oxygen with metals [4]. Extensive experiments have been carried out on these systems, e.g. dissociative and non-dissociative adsorption, dependence on temperature, coverage and azimuthal dependence [5–20]. In the oxygen on Ag, Pd and Pt surfaces for example, superoxide (O_2^-) and peroxides (O_2^{2-}) adsorbed states have been observed [21–40]. For the O_2–Cs system, emission of exoelectrons and O^- was observed in the gas phase [17–20]. For the O_2–Al system, atomic oxygen is found to be adsorbed to the surface at 80 Å intervals [13–15]. See Fig. 1. An explanation given to such baffling findings is a dissociation via Coulomb explosion causing a ballistic course of one of the oxygen atoms due to a double electron transfer from the metal to the molecule, and the formation of a very strong atom–surface bond. The current experimental findings and a theoretical static charge transfer analysis have recently been review by Greber [41].

In this paper the quantum dynamics of the oxygen–metal encounter is studied for three metals that differ in their electronic properties. These properties can either stabilize charged species on the surface, dissociate the oxygen or emit charge species back to the gas phase.

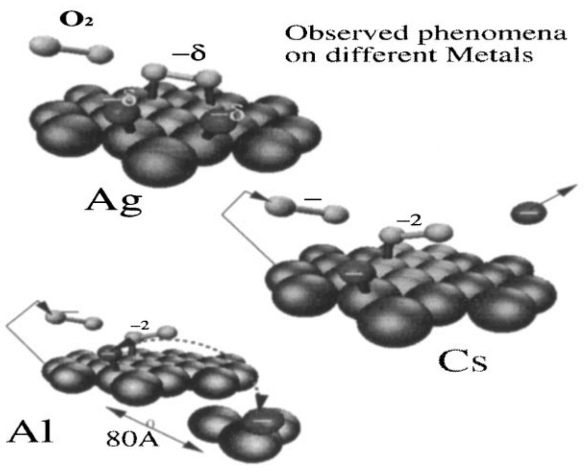

Fig. 1. Three different oxygen charge transfer species on various metals. Notice the formation of adsorbed O_2^-, O_2^{2-} and O^- and the emission of electrons.

The approach of the present study is to construct a quantum mechanical dynamical model of these processes. The dynamics takes place on a set of four semi-empirical diabatic potentials, constructed using results of ab initio calculations and experimental data. A universal functional form was employed which allows comparison between different metals. The dynamics was solved by propagation of an initial wave function emerging from the gas phase. The appearance of the products was then analyzed in terms of the integrated flux in each of the reaction channels.

The main goal of this study is to investigate the dynamics of non-adiabatic charge transfer transitions. As a model system, the encounter of molecular oxygen with metal surfaces is investigated. Hence, as the metals are mainly considered as electron donors their structural details are omitted. The emphasis is on direct scattering events that are fast relative to the time scale of energy dissipation. The study of the equilibration of the long-lived intermediates can be dealt with [42–44] and is postponed to a future study.

2. Description of the model

2.1. Potential energy surfaces

The construction of universal potential energy surfaces for the oxygen–metal systems is based on an empirical approach. In this approach the ab initio results, together with available experimental data, are used to parametrize universal diabatic potentials.

When oxygen in the gas phase approaches a surface a series of charge transfer events can take place:

$$(O_2)_{gas} \rightarrow (O_2)_{ad} \rightarrow O_2^{1-} \rightarrow O_2^{2-} \rightarrow 2O^- . \qquad (1)$$

Hence, at least four potential energy surfaces are required to describe these species: O_2 physisorption, O_2^- (superoxide), O_2^{2-} (peroxide) and $2O^-$ (dissociated oxygen). These potential energy surfaces were adjusted to gas-phase experimental energies of O_2, O, O^- and O_2^- for large particle–surface distances. Close to the metal surface the potentials were adjusted to the calculations of

Nakatsuji and Nakai [45–48] for oxygen on silver and to experimental results by Kleyn and coworkers [9–12]. Density functional theory calculations were also performed on these systems [49–52]. However, these are not employed here since, by construction, they give only the lowest adiabatic potential.

Since in this study the metals are mainly considered as electron donors, the potentials for the oxygen–cesium and oxygen–aluminum systems were obtained by scaling the parameters of the oxygen–silver system. This scaling accounts for the different work functions, and the experimental observations for Al [13–15], and Cs [17–20].

2.1.1. Physisorption potential

A gas-phase oxygen molecule correlates to a non-bonding O_2 on the metal surface, which is the physisorption state. The forces operating on the molecule are dispersion forces. To a first approximation, these forces are universal and are the result of the attraction between the polarization of the molecule and its image charge distribution in the metal. The physical picture of the physisorbed state is of an oxygen molecule whose internal degrees of freedom are only slightly perturbed, i.e. an almost freely rotating and vibrating molecule. This state is characterized by a very low molecule–surface vibrational frequency.

The dependence of the physisorption potential, at most collision energies, on the orientation angles θ and ϕ can be neglected. Only at very low temperatures does the anisotropic part of the polarization become important, where it causes a preferential perpendicular orientation. The following functional form has been chosen to describe the physisorption potential:

$$V_g(r, z, \theta) = A_g\, e^{-b_g z} - \frac{C_g(\theta)}{z^3}[1 - \Gamma_4(z, 0, 2b_g)] + D_g\{1 - e^{-\alpha_{O\text{–}O}(z)[r - r_e(z)]}\}^2 \qquad (2)$$

where z is the distance of the molecular center of mass from the surface plane of the metal, r is the molecular inter-nuclear distance and θ is the orientation angle measured from the surface normal. The dependence of $C_g(\theta)$ can be described as $C_g(\theta) = C_g^0 + C_g^2 P_2[\cos(\theta)]$. In the following a flat surface is assumed; therefore, the azimuthal dependence is neglected. The incomplete Gamma function Γ is used as an interpolation function from the gas-phase values to the adsorbed values:

$$\Gamma_m(z, z_0, a) = \sum_{k=0}^{k=m} \frac{a(z - z_0)k}{k!}\, e^{-a(z - z_0)}. \qquad (3)$$

The molecular parameters become

$$\alpha_{O\text{–}O}(z) = \alpha_{O\text{–}O}^{ad} \text{ for } z < z_e \qquad (4)$$

$$\alpha_{O\text{–}O}(z) = \alpha_{O\text{–}O}^{g} - (\alpha_{O\text{–}O}^{g} - \alpha_{O\text{–}O}^{ad})\Gamma_4(z, z_e, b_g)$$

for $z > z_e$

and

$$r_e(z) = r_e^g = (r_e^g - r_e^{ad})\Gamma_4(z, z_e, b_g). \qquad (5)$$

The last term in Eq. (2) represents the molecular potential where the parameters are obtained by interpolation between the values of the gas phase and the adsorbate. In addition, the potential should be fitted to reproduce the O_2–surface vibrational frequency and the adsorption energy. In this potential form the plane where $z = 0$ is somewhat arbitrary. Physically it represents the plane where the gradient in electron density is maximized when going from the bulk of the metal into the gas phase. Since the source of the physisorption potential is the dispersion forces, it has a universal character that depends only on the polarization properties of the molecule. As a result, scaling relations exist between the gas-phase polarization and the surface potential parameters. These scaling relations are used to check the consistency of the potential parameters used in the calculation [53]. The consequence is that the same physisorption parameters were used for all metals (Fig. 2).

2.1.2. Charged intermediates

Two candidates have been suggested for the charged intermediate molecular species. The first is the superoxide O_2^- and the second is the peroxide species O_2^{2-}. The intermediate states are expected have a much stronger binding energy to the metal than the physisorption state, resulting in an increase in the oxygen–metal vibrational frequency. Owing to the partial charge transfer from the metal to the molecule the O–O bond in the

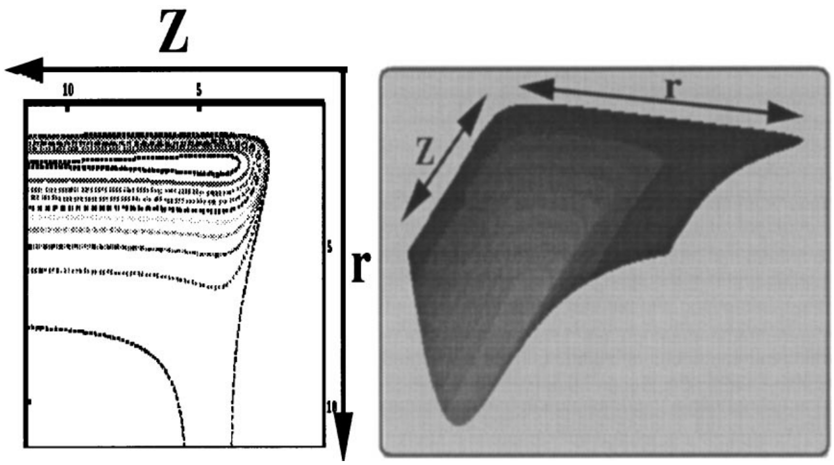

Fig. 2. The physisorption potential surface for all metals as a function of *z* the distance from the surface and *r* the interatomic distance. Notice the shallow attractive well at distance of 4.7 Å from the surface.

charged intermediate is weakened and stretched. As a result the O–O vibration frequency is reduced compared with its value in the gas phase. The typical vibrational O–O frequency of the superoxide species is in the range 950–1100 cm^{-1} and for the peroxide 600–700 cm^{-1}. These potentials are expected to exhibit strong orientation dependence where a flat geometry, i.e. $|\theta| = \pi/2$, is preferable.

The functional form chosen to describe the charged intermediate states is a combination of direct binding represented by a Morse potential and a Coulomb interaction with the image charge in the metal. Thus the potential for the superoxide (Fig. 3) has the form

$$V_{\mathrm{m}}(r, z) = A_m^{(\mathrm{M{-}O_2^-})}[1 - \mathrm{e}^{-\alpha_{\mathrm{M{-}O_2^-}}(r)(z - z_e)}]^2 - \frac{Z_{\mathrm{efc}}^{\mathrm{super}}(z)}{2z}[1 - \Gamma_2(z, 0, 2b_{\mathrm{m}})] + D_{\mathrm{a}}^{(\mathrm{O{-}O^-})} \{1 - \mathrm{e}^{-\alpha_{\mathrm{O{-}O^-}}(z)[r - r_{\mathrm{e}}(z)]}\}^2 + E_{\mathrm{m}} - E_{\mathrm{a}}(\mathrm{O_2}), \tag{6}$$

where the parameter $A_{\mathrm{m}}^{(\mathrm{M{-}O_2^-})}$ represents the molecule–metal direct bond strength, and $D_{\mathrm{a}}^{(\mathrm{O{-}O^-})}$ the

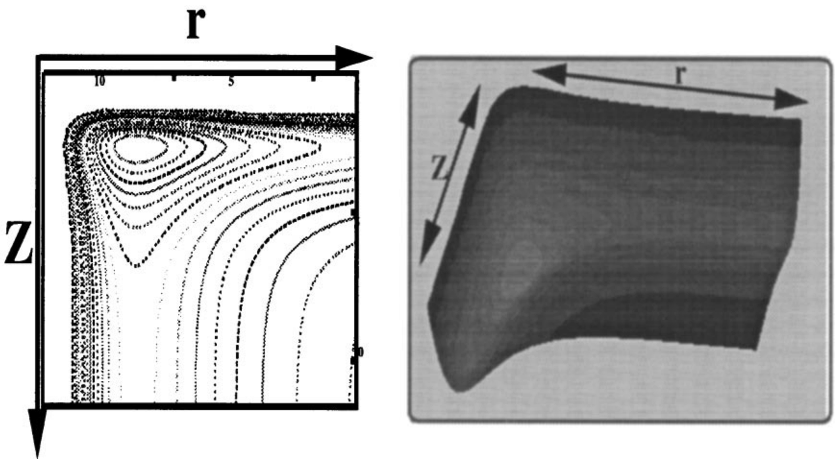

Fig. 3. The superoxide potential for the O_2–Cs system. The well depth is 1.11 eV relative to the physisorption state.

oxygen–oxygen bond strength in the superoxide. The effective charge $Z_{\mathrm{efc}}^{\mathrm{super}}$ represents the amount of charge transferred from the metal to the adsorbate. This charge is reduced from the value of O_2^{1-} in the gas phase to $O_2^{0.54-}$ for the adsorbate as obtained in the ab initio calculations [45–48]. Similarly, the Morse parameters representing the oxygen–oxygen bonding are interpolated from their gas-phase values to the corresponding values in the adsorbed state. The last two quantities in Eq. (6), E_{m} and $E_{\mathrm{a}}(O_2)$, are the work function of the metal and the electron affinity of the oxygen molecule respectively.

The same functional form describes the peroxide species, where the parameters were adjusted accordingly. All the parameters are summarized in Tables 1–3. The peroxide potential is shown in Fig. 4.

2.1.3. The dissociative potential

The binding between the atomic oxygen ion and the metal is described by a combination of a covalent contribution described by a Morse potential together with an ionic part described by a Coulomb interaction between the ion and its image charge. The interaction between the two oxygen ions is the direct Coulomb repulsion and the Coulomb attraction to the image charge of the other ion:

$$V_{\mathrm{diss}}(z,r)-2A_{\mathrm{m}}^{(\mathrm{M\text{–}O}^-)}[1-\mathrm{e}^{-\alpha_{\mathrm{M\text{–}O}^-}(z)(z-z^{\mathrm{e}})}]^2 - \frac{2Z_{\mathrm{efc}}^{\mathrm{atom}}(z)}{2z}[1-\Gamma_2(z,0,2b_{\mathrm{m}})]+\frac{2Z_{\mathrm{efc}}^{\mathrm{atom}}(z)}{r} - \frac{2Z_{\mathrm{efc}}^{\mathrm{atom}}}{\sqrt{r^2+4z^2}}+2E_{\mathrm{m}}-2E_{\mathrm{a}}^{\mathrm{atom}}, \qquad (7)$$

see Fig. 5.

2.1.4. Charge transfer

At large particle–metal distances each one of these potentials is shifted energetically relative to the physisorbed potential (see Fig. 6). The magnitude of the shift is determined by the difference between the value of the metal work function E_{m} and the particle electron affinity E_{a}. In all potentials the effective charge on the adsorbate is interpolated from its gas-phase value to its value on the metal:

$$Z_{\mathrm{efc}}(z)=Z_{\mathrm{efc}}^{\mathrm{ad}} \text{ for } z<z_{\mathrm{e}} \qquad (8)$$

$$Z_{\mathrm{efc}}(z)=Z_{\mathrm{efc}}^{\mathrm{g}}-(Z_{\mathrm{efc}}^{\mathrm{g}}-Z_{\mathrm{efc}}^{\mathrm{ad}})(1-\mathrm{e}^{-\gamma/z})$$

for $z>z_{\mathrm{e}}$.

For silver the value of $Z_{\mathrm{efc}}^{\mathrm{ad}}$ was taken from the ab initio calculations of Refs. [45,46]. In this embed-

Table 1
Parameters of the oxygen–silver potential (energy in electron-volts; distance in ångströms)

Physisorption	$A_{\mathrm{g}}=829$	$C_{\mathrm{g}}=4.2$	$D_{\mathrm{g}}=5.1$	
	$b_{\mathrm{g}}=3.73$	$\alpha_{\mathrm{O\text{–}O}}^{\mathrm{ad}}=2.63$	$\alpha_{\mathrm{O\text{–}O}}^{\mathrm{g}}=2.69$	
	$r_{\mathrm{e}}^{\mathrm{g}}=1.208$	$r_{\mathrm{e}}^{\mathrm{ad}}=1.24$	$z_{\mathrm{e}}=2.47$	
Superoxide	$A_{\mathrm{m}}^{(\mathrm{M\text{–}O_2^-})}=4.8$	$D_{\mathrm{a}}^{\mathrm{O\text{–}O^-}}=4.1$	$E_{\mathrm{m}}=4.65$	$E_{\mathrm{a}}^{O_2}=0.46$
	$b_{\mathrm{m}}=3.56$	$\alpha_{\mathrm{M\text{–}O_2^-}}=0.7$	$\alpha_{\mathrm{O\text{–}O^-}}=1.74$	
	$r_{\mathrm{e}}=1.55$	$Z_{\mathrm{efc}}^{\mathrm{super}}=-0.54$	$Z_{\mathrm{efc}}^{\mathrm{g}}=-1$	$z_{\mathrm{e}}=2.6$
Peroxide	$A_{\mathrm{m}}^{(\mathrm{M\text{–}O_2^{2-}})}=5.4$	$D^{(\mathrm{O^-\text{–}O^-})}{}_{\mathrm{a}}=3.9$	$E_{\mathrm{m}}=4.65$	
	$b_{\mathrm{m}}=3.76$	$\alpha_{\mathrm{M\text{–}O_2^{2-}}}=0.917$	$\alpha_{\mathrm{O^-\text{–}O^-}}=1.174$	$\gamma=0.6$
	$r_{\mathrm{e}}=1.66$	$Z_{\mathrm{efc}}^{\mathrm{per}}=-1.4$	$Z_{\mathrm{efc}}^{\mathrm{g}}=-2$	$z_{\mathrm{e}}=2$
Dissociation	$A_{\mathrm{m}}=4$	$D_{\mathrm{m}}=3.9$	$E_{\mathrm{m}}=4.65$	$E_{\mathrm{a}}^{O_2^-}=1.46$
	$b_{\mathrm{m}}=3.56$	$\alpha_{\mathrm{M\text{–}O}}^{\mathrm{ad}}=0.9$		
		$Z_{\mathrm{efc}}^{\mathrm{g}}=-1$	$Z_{\mathrm{efc}}^{\mathrm{ad}}=-0.79$	$z_{\mathrm{e}}=2$

Table 2
Parameters of the oxygen–cesium potential (energy in electron-volts; distance in ångströms)

Physisorption	$A_g = 829$	$C_g = 4.2$	$D_g = 5.1$	
	$b_g = 3.73$	$\alpha^{ad}_{O\text{–}O} = 2.63$	$\alpha^{g}_{O\text{–}O} = 2.69$	
	$r^g_e = 1.208$	$r^{ad}_e = 1.24$	$z_e = 2.47$	
Superoxide	$A_m^{(M\text{–}O_2^-)} = 2.2$	$D_a^{O\text{–}O^-} = 4.1$	$\mathrm{E}_m = 1.8$	$E_a^{O_2} = 0.46$
	$b_m = 3.56$	$\alpha_{M\text{–}O_2^-} = 0.7$	$\alpha_{O\text{–}O^-} = 1.74$	
	$r_e = 1.49$	$Z^{super}_{efc} = -0.9$	$Z^g_{efc} = -1$	$z_e = 2.4$
Peroxide	$A_m^{(M\text{–}O_2^{2-})} = 2.4$	$D^{(O^-\text{–}O^-)}{}_a = 3.9$	$E_m = 1.8$	
	$b_m = 3.76$	$\alpha_{M\text{–}O_2^{2-}} = 0.917$	$\alpha_{O^-\text{–}O^-} = 1.174$	$\gamma = 0.6$
	$r_e = 1.56$	$Z^{per}_{efc} = -1.8$	$Z^g_{efc} = -2$	$z_e = 2$
Dissociation	$A_m = 6$	$D_m = 3.9$	$E_m = 1.8$	$E_a^{O} = 1.46$
	$b_m = 3.56$	$\alpha^{ad}_{M\text{–}O} = 0.9$		
		$Z^g_{efc} = -1$	$Z^{ad}_{efc} = -0.9$	$z_e = 2$

Table 3
Parameters of the oxygen–aluminum potential (energy in electron-volts; distance in ångströms)

Physisorption	$A_g = 829$	$C_g = 4.2$	$D_g = 5.1$	
	$b_g = 3.73$	$\alpha^{ad}_{O\text{–}O} = 2.63$	$\alpha^{g}_{O\text{–}O} = 2.69$	
	$r^g_e = 1.208$	$r^{ad}_e = 1.24$	$\mathrm{z}_e = 2.47$	
Superoxide	$A_m^{(M\text{–}O_2^-)} = 4.8$	$D_a^{O\text{–}O^-} = 4.1$	$E_m = 4.4$	$E_a^{O_2} = 0.46$
	$b_m = 3.56$	$\alpha_{M\text{–}O_2^-} = 0.7$	$\alpha_{O\text{–}O^-} = 1.74$	
	$r_e = 1.55$	$Z^{super}_{efc} = -0.9$	$Z^g_{efc} = -1$	$z_e = 1.9$
Peroxide	$A_m^{(M\text{–}O_2^{2-})} = 5.4$	$D^{(O^-\text{–}O^-)}{}_a = 3.9$	$E_m = 4.4$	
	$b_m = 3.76$	$\alpha_{M\text{–}O_2^{2-}} = 0.917$	$\alpha_{O^-\text{–}O^-} = 1.174$	$\gamma = 0.6$
	$r_e = 1.66$	$Z^{per}_{efc} = -1.8$	$Z^g_{efc} = -2$	$z_e = 2.22$
Dissociation	$A_m = 7$	$D_m = 3.9$	$E_m = 4.4$	$E_a^{O_2^-} = 1.46$
	$b_m = 3.56$	$\alpha^{ad}_{M\text{–}O} = 0.9$		
		$Z^g_{efc} = -1$	$Z^{ad}_{efc} = -0.9$	$z_e = 2$

ded cluster method, the charge transfer from the bulk of the metal is adjusted by an effective ‘chemical potential’ of the free electrons. For the other metals the value of Z^{ad}_{efc} was scaled by the ratio of their work functions to that of silver.

2.1.5. The non-adiabatic coupling potential

The non-adiabatic coupling between each pair of states weights the possibility of a charge transfer event. The coupling term is therefore chosen to be proportional to the electron density. The electron

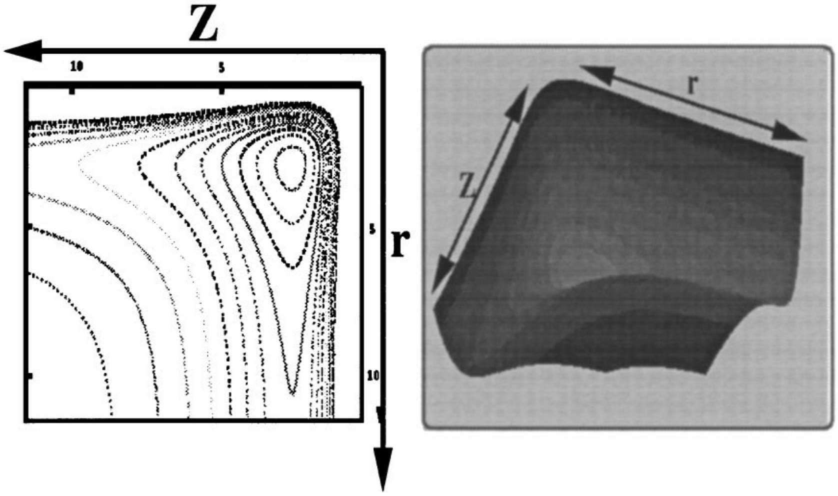

Fig. 4. The peroxide potential surface for the O_2–Cs system. The well depth is 2.07 eV relative to the physisorption state.

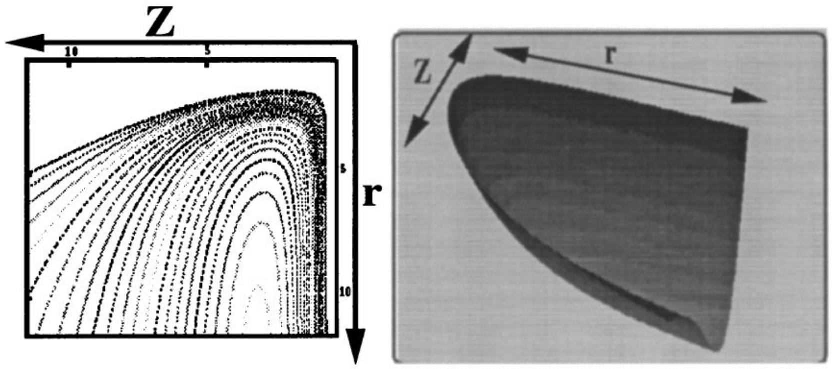

Fig. 5. The dissociative chemisorption potential surface for the O_2–Cs system.

density decays exponentially in the classically forbidden region outside the metal into the vacuum. The decay parameter is estimated using the metal work function and the effective charge difference.

$$V_{\mathrm{int}}(z,r)=A_{\mathrm{ab}}\,\mathrm{e}^{-\alpha_{\mathrm{int}}(z/\hbar)}\,\mathrm{e}^{(r-r_{\mathrm{eq}})^2} \tag{9}$$

where the decay parameter is given by

$$\alpha_{\mathrm{int}}=\sqrt{\frac{-2(E_{\mathrm{m}})|Z^{\mathrm{a}}_{\mathrm{efc}}-Z^{\mathrm{b}}_{\mathrm{efc}}|}{m_{\mathrm{e}}e}}$$

and where Z^{i}_{efc} is the effective charges of each species. A_{ab} is the interaction matrix element. In the region of small coupling, which is relevant for this study, the transition from one surface to the other is proportional to $|A_{\mathrm{ab}}|^2$. A_{ab} was assigned the value of 0.1 eV in all calculations, but, since the direct reaction product yields are scaled by this value, A_{ab} can be readjusted to fit experimental yields of O_2^- when they become available (see Fig. 8).

2.1.6. *Potential summary*

The differences between metals in this model are due to the variations in the work functions and heats of adsorption for the different species. For metals with low work functions the non-adiabatic coupling potential becomes long range. This difference can change the dissociation mecha-

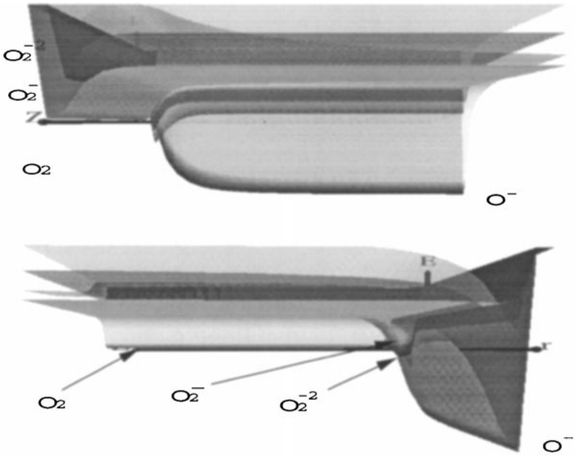

Fig. 6. Two different viewpoints of the diabatic potentials for the O_2–Cs system. Notice the crossing seams between the different potentials and the different asymptotic values of the potentials.

nisms significantly, leading to a harpooning mechanism of long-range charge transfer for metals with low values of work functions.

2.2. Propagation

The dynamics of the charge transfer process were followed by solving the multi-channel time-dependent Schrödinger equation. The method of solution was to represent the wave function on a grid. The grid parameters (see Table 4) were set to accommodate the energy involved in the process and contain the volume where the non-adiabatic encounters take place [54,55]. First, the initial wave function representing a free oxygen molecule in the gas phase was calculated [56]. This wave function was then propagated in time using the Chebychev scheme [54]. Analysis of the process was carried out by integrating the flux passing into each of the possible asymptotic channels [57].

The high energy involved and the long-range interaction forces mean that very large grids have to be used, resulting in heavy computational demands. To minimize the computation, the analysis of the ion production was carried out before the asymptotic region had been reached. This was done by filtering out that part of the wave function

Table 4
Typical grid parameters and time steps

npz	640
d*z* (Å)	0.009
npr	128
d*r* (Å)	0.02
d*t* (au)	10

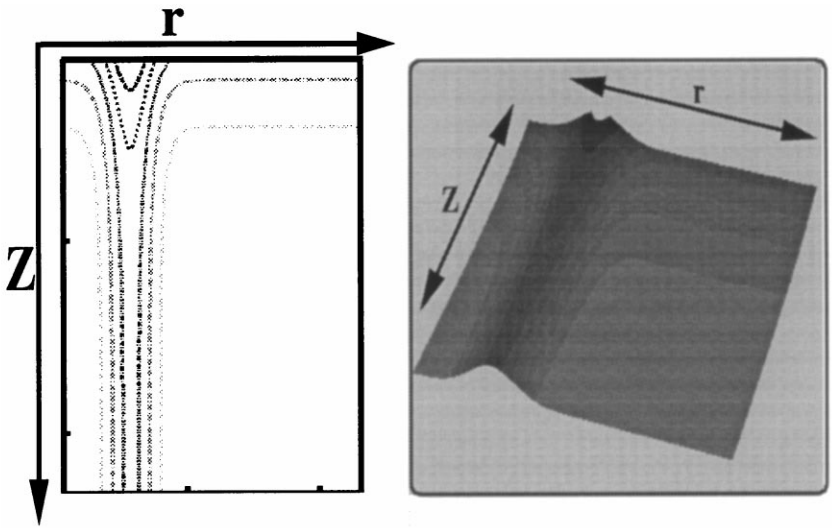

Fig. 7. The couplings potential between physisorption potential and the superoxide potential for O_2/Cs. The other couplings potentials have a similar form.

which had sufficient energy to reach the asymptotic region. The procedure was checked in one-dimensional calculations and resulted in an accuracy of better than 2%.

2.2.1. Time evolution

The propagation starts with the wave function far from the surface. The initial wave function is a product of a Gaussian wave function in the translational z coordinate and vibrational eigenstate in the direction of r as shown in Fig. 8. As time progresses the wave packet splits into the different electronic surfaces.

The two deep potential wells corresponding to the peroxide and superoxide cause long resident times of the wave function near the surface. Eventually, the wave packet will find its way to the energetically allowed asymptotic channels. A time scale separation is observed between the direct inelastic scattering and the trapped wave function with long residence time. Employing this observation, a separate asymptotic analysis is performed on the two parts. The flux leading to asymptotic products is integrated along a perpendicular flux surface, as shown in Fig. 9. The integration time is carefully chosen to include the direct part and exclude the indirect part.

3. Results and discussion

The accumulated flux of the direct scattering part into the different asymptotic channels for three metals and two initial O_2 vibrational states is shown in Fig. 10.

Insight into the results presented by Fig. 10 is obtained by following the oxygen–metal encounter sequentially. The role of the different parts of the crossing seam in determining the outcome has been checked by turning off different parts of the non-adiabatic coupling potential and repeating the dynamical calculation. An enhanced transition probability is always found when the classical turning point region matches the crossing seam.

The oxygen molecule approaches the metal from the gas phase on the physisorption potential, which

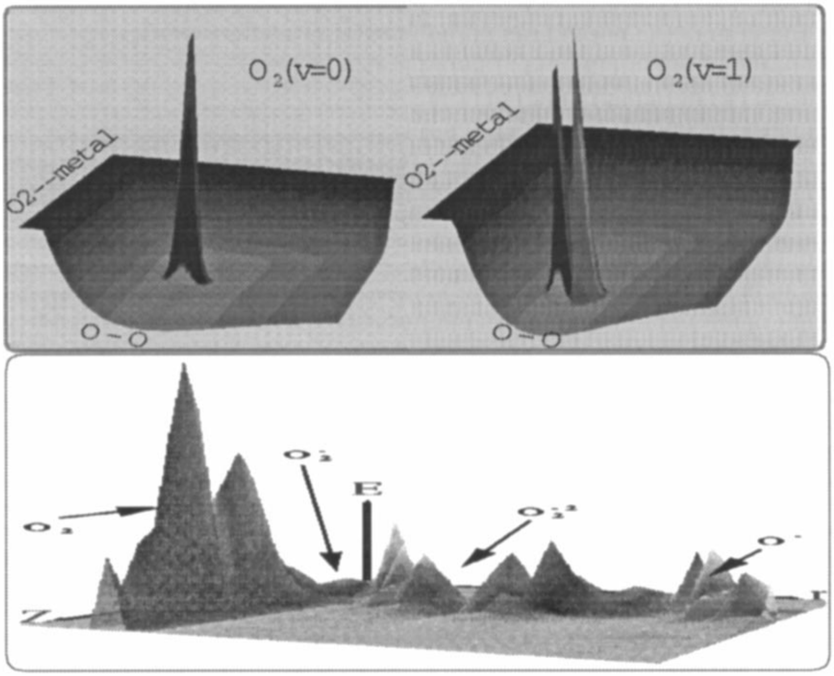

Fig. 8. The initial absolute square of the wave function $|\psi(z, r, t=0)|^2$ (above) and the coordinate projections of the different oxygenic species after 500 fs (below).

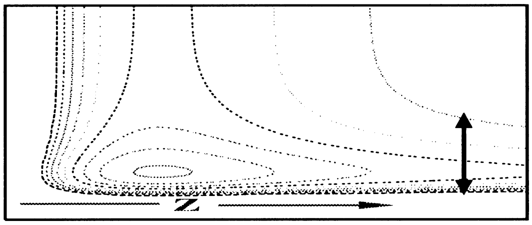

Flux dividing surface for the super—oxide ejection chanel

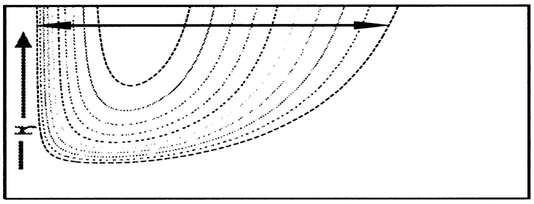

flux dividing surface of the dissociation channel

Fig. 9. The flux surfaces leading to dissociation or to superoxide ejection into the gas phase superimposed on the appropriate diabatic potentials.

is almost flat relative to the high kinetic energy involved. The first encounter is with the superoxide potential. Fig. 11 displays the crossing seams between the physisorption state and the other three potential surfaces. For the oxygen–cesium encounter the physisorption–superoxide seam extends far into the asymptotic region, allowing a long-range harpooning mechanism which is operative even at a very low incident kinetic energy. At short oxygen–surface distances, the seam changes direction and bifurcates. This fact is reflected in a dip in the probability of non-reactive ejection of oxygen at ~4 eV where there is a kink in the direction of the seam. This dip is not observed in the $v=1$ initial state because of the position of the kink in the seam relative to the nodal plane of the $v=1$ state. As a result, the $v=1$ is significantly less reactive than the $v=0$ state.

For oxygen on the aluminum surface the reaction dynamics are the result of an interplay between the crossing seams of the physisorption and the superoxide and the peroxide surfaces. This convoluted potential-crossing scenario enhances the trapping probability. The dip of the $v=1$ initial state near 3 eV is the result of the kink in the peroxide seam, which matches the maximum in the amplitude of this state. The dip in the $v=0$ initial state occurs at the energy value where the two seams cross.

The main observed feature in the superoxide emission is the energy threshold, which is determined by the work-function of the metal. For the $v=0$ Cs system the superoxide production decreases after the threshold point, reflecting the decrease in the harpooning probability with increasing kinetic energy. The increase in superoxide production from 3.5 eV is the result of the kink in the seam. The lower panel shows the direct oxygen dissociation channel. The values for all metals are very small, pointing to the fact that the dissociation is a delayed process that feeds on the trapped oxygen species close to the metal.

The influence of the initial vibrational excitation on the direct reaction channels is shown in Fig. 12. For the O_2–Cs system, at lower energies the position of the seam approximately in the middle of the physisorption entrance channel is reflected by the even alternations of the final vibrational distribution. These alternations depend on the initial vibrational state and reflect a propensity for $\Delta v \pm 2$ transitions. At higher translational energies, when the relevant seam becomes perpendicular to the motion, the final vibrational distribution becomes almost independent of the initial vibrational state. For the ejected superoxide at translational energy of 3 eV the distribution is again independent of the initial vibration. This is also true for the O_2–Ag system. The reason for this phenomenon is that there is sufficient time even for the direct ejection channel to scramble the energy between the different vibrations. At higher collision energies of ~4.5 eV, significant vibrational excitation occurs. The O_2–Al system has a different non-adiabatic crossing structure, which is reflected in the final vibrational distribution.

4. Summary

Charge transfer phenomena in gas–surface encounters have been studied extensively, both experimentally and theoretically [41]. Nevertheless, there has been almost no work on the

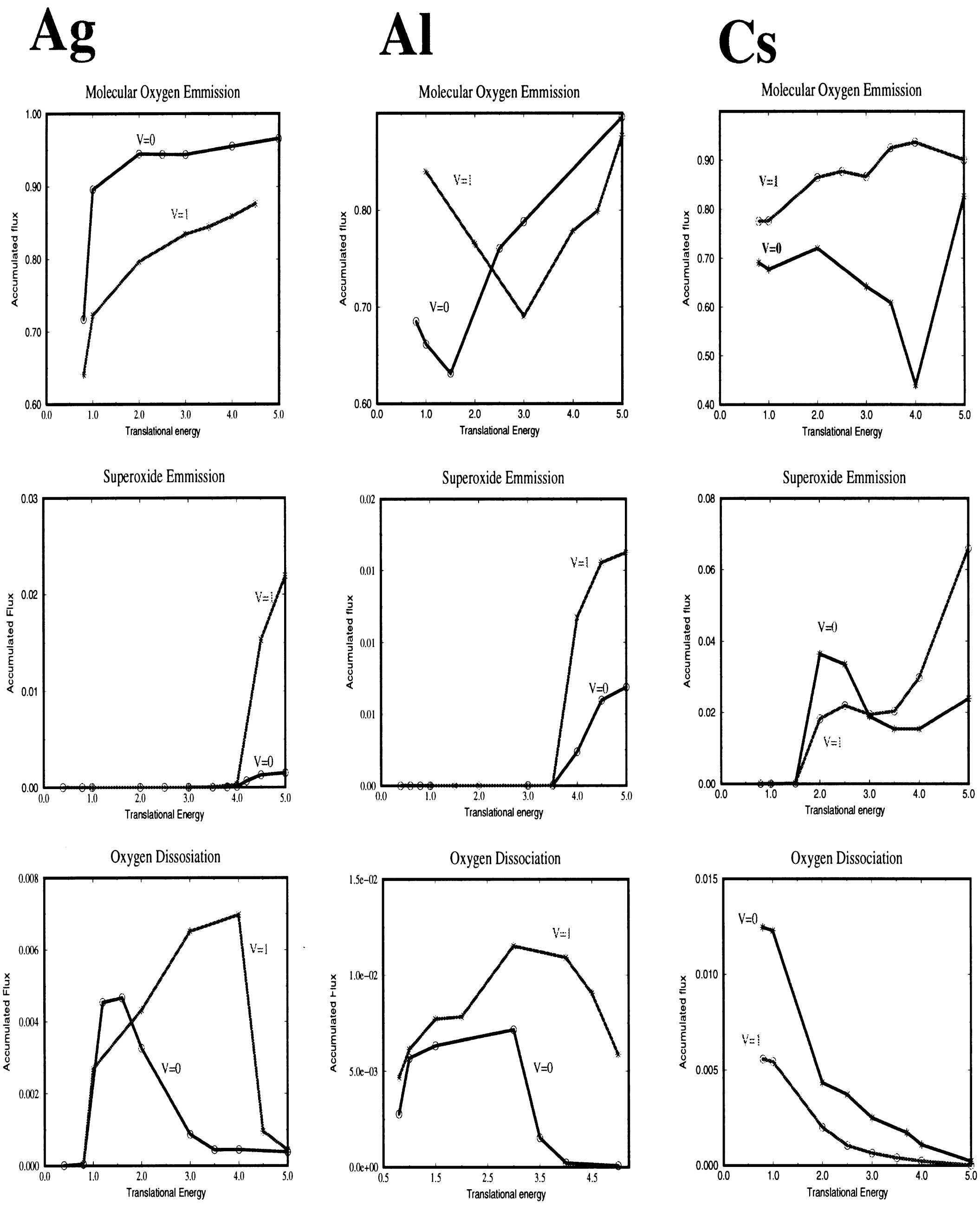

Fig. 10. The accumulated flux with respect to initial vibrational and translational energy at the three reaction channels for the various different metals: Ag in the left column, Al in the middle and Cs in the right column. Ejected molecular oxygen to the gas phase is shown in the top row, ejected superoxide in the middle row and dissociation yield in the bottom row.

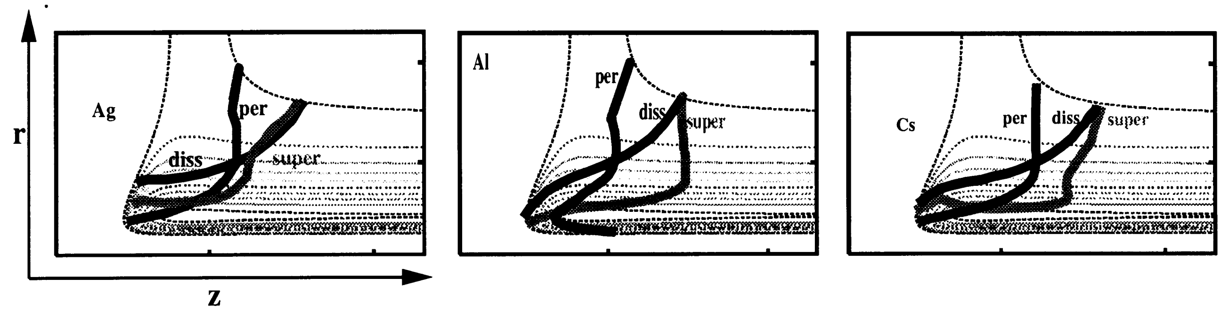

Fig. 11. The crossing seams between the physisorption potential and the other potentials for the three metals superimposed on the physisorption potential.

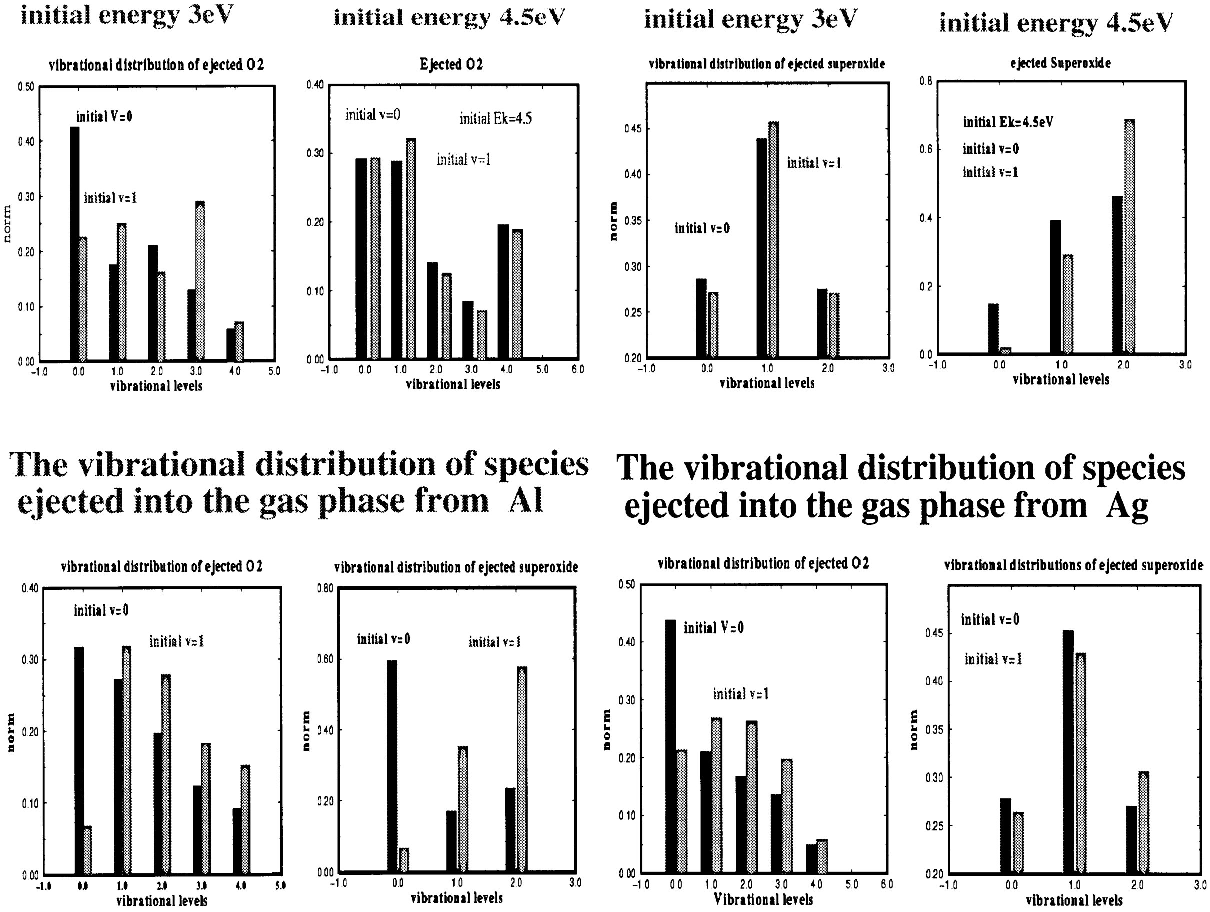

Fig. 12. The vibrational distribution of molecules emitted into the gas phase as superoxide (right) and molecular oxygen (left). The gray histograms are attributed to the $v=1$ initial state.

quantum dynamical aspects of these processes. The purpose of this paper is to link experimental observables to the details of the non-adiabatic dynamics.

The dynamics of the oxygen–metal systems can be generally partitioned into direct and indirect parts. The existence of deep potential wells of the superoxide and peroxide species on the surface and energy dissipation on the surface can create long-lived trapped states. Nevertheless, at high impact energies a large portion of the oxygen molecules is reflected back. The amount of the reflected oxygen depends on the nature of the non-adiabatic transition. The topology of the crossing seam is responsible for the non-monotonic energy dependence of the reaction yields. Therefore, it is not surprising that low dissociation yields can be obtained much above the energy of the crossing seams.

The possibility of observing the oxygen molecular ion O_2^- in the gas phase depends on the existence of a direct channel. At the energies above the threshold of creation of O_2^- such a direct channel has been calculated. The yields of this species are crucially dependent on the topology of seams between the different potential energy surfaces. This topology can be influenced by changing the work function of the metals or by employing singlet oxygen $^1\Sigma_g^+$, which reduces the threshold for O_2^- production by 1.8 eV. Work in this direction is in progress [58].

Acknowledgements

This research was supported by the German–Israel Foundation (GIF). The Fritz Haber Research Center is supported by the Minerva Gesellschaft für die Forschung, GmbH München, FRG.

References

[1] B. Kasemo, Phys. Rev. Lett. 32 (1974) 1114.
[2] J. Stromquist, L. Hellberg, B. Kasemo, B.I. Lundqvist, Surf. Sci. 352 (1996) 354.
[3] L. Hellberg, J. Stromquist, B. Kasemo, B.I. Lundqvist, Phys. Rev. Lett. 74 (1995) 4742.
[4] A.W. Kleyn, The Physics of Electronic and Atomic Collisions, FOM Institute, Amsterdam, 1978, p. 451.
[5] L. Vattoune, M. Rocca, C. Boragno, U. Valbusa, Initial sticking coefficient of O_2 on Ag (110), J. Chem. Phys. 101 (1994) 713.
[6] L. Vattuone, M. Rocca, C. Boragno, U. Valbusa, Coverage dependence of sticking coefficient of O_2 on Ag (110), J. Chem. Phys. 101 (1994) 726.
[7] L. Vattuone, C. Boragno, M. Pupo, P. Restelli, M. Rocca, U. Valbusa, Azimuthal dependence of sticking probability of O_2 on Ag, Phys. Rev. Lett. 72 (1994) 510.
[8] A. Raukema, D.A. Batler, F.M.A. Box, A.W. Kleyn, J. Chem. Phys. 101 (1994) 713.
[9] A. Raukema, Ph.D. thesis, 1995; J. Chem. Phys. 101 (1994) 726.
[10] P.H. Reijnen, A. Raukema, U.van Flooten, A.W. Kleyn, J. Chem. Phys. 94 (1991) 2368.
[11] M.E.M. Spruit, A.W. Kleyn, Chem. Phys. Lett. 159 (1989) 342.
[12] M.E.M. Spruit, Ph.D. thesis, 1988; Phys. Rev. Lett. 72 (1994) 510.
[13] I.P. Batra, L. Kleinman, J. Electron Spectrosc. Relat. Phenom. 33 (1984) 175.
[14] P.S. Bagus, C.R. Brundle, F. Illas, F. Parmigiani, G. Polzonetti, Phys. Rev. B 44 (1991) 9025.
[15] H. Brune, J. Wintterlin, R.J. Behm, G. Ertl, Phys. Rev. Lett. 68 (1991) 624.
[16] L. Osterlund, I. Zoric, B. Kasemo, Phys. Rev. B 55 (1997) 15452.
[17] T. Greber, R. Grobecker, A. Morgante, A. Bottcher, G. Ertl, Phys. Rev. Lett. 70 (1992) 1331.
[18] A. Bottcher, A. Morgante, T. Giebel, T. Greber, G. Ertl, Chem. Phys. Lett. 231 (1994) 119.
[19] R. Grober, H. Shi, H. Bldau, T. Hertel, T. Greber, A. Bottcher, K. Jacobi, G. Ertl, Phys. Rev. Lett. 72 (1993) 578.
[20] A. Bottcher, R. Imbeck, A. Morgante, G. Ertl, Phys. Rev. Lett. 65 (1990) 2035.
[21] R.B. Grant, R.M. Lambert, Surf. Sci. 146 (1984) 256.
[22] C.T. Campbell, Surf. Sci. 157 (1985) 43.
[23] C.T. Campbell, Surf. Sci. 173 (1986) L641.
[24] F. Besenbacher, J.K. Norskov, Prog. Surf. Sci. 44 (1993) 5.
[25] C. Backx, C.P.M. de Groot, P. Biloen, Surf. Sci. 104 (1981) 300.
[26] C. Pettenkofer, J. Eikmans, U. Erturk, A. Otto, Surf. Sci. 151 (1985) 9.
[27] B.A. Sexton, R.J. Madix, Chem. Phys. Lett. 76 (1980) 294.
[28] D.A. Outka, J. Stohr, W. Jark, P. Stevens, J. Solomon, R.J. Madix, Phys. Rev. B 33 (1987) 4119.
[29] T.H. Upton, P. Stevens, F.J. Madix, J. Chem. Phys. 88 (1988) 3988.
[30] C. Pettenkofer, I. Pockrand, A. Otto, Surf. Sci. 135 (1983) 52.
[31] P.V. Kamath, K. Prabhakaran, C.N.R. Rao, J. Chem. Soc. Chem. Commun. (1987) 715.

[32] M.A. Barteau, R.J. Madix, Surf. Sci. 97 (1980) 101.
[33] A. Puschmann, J. Haase, Surf. Sci. 144 (1984) 559.
[34] D. Schmeisser, J.E. Demuth, Ph. Avouris, Phys. Rev. B 26 (1982) 4857.
[35] K. Bange, T.E. Madey, J.K. Sass, Chem. Phys. Lett. 113 (1985) 56.
[36] M. Dean, A. McKee, M. Bowker, Surf. Sci. 211 (1989) 1061.
[37] A.J. Capote, J.T. Roberts, R.J. Madix, Surf. Sci. 209 (1992) L151.
[38] A.I. Boronin, V.I. Buchtiyarov, A.L. Vishnevskii, G.K. Boreskov, V.I. Savchenko, Surf. Sci. 201 (1988) 195.
[39] V.I. Bukhtiyarov, A.I. Boronin, V.I. Savchenko, Surf. Sci. 232 (1990) L205.
[40] L. Vattuone, M. Rocca, U. Valbusa, Anharmonic shift in the stretching frequency of O_2 chemisorbed on Ag (110), Surf. Sci. 314 (1994) L904.
[41] T. Greber, Surf. Sci. Rep. 28 (1997) 1.
[42] P. Saalfrank, R. Baer, R. Kosloff, Density matrix description of laser-induced hot electron mediated photodesorption, Chem. Phys. Lett. 230 (1994) 463.
[43] P. Saalfrank, R. Baer, R. Kosloff, (1996)
[44] R. Baer, R. Kosloff, Quantum dissipative dynamics of adsorbates near metal surfaces: a surrogate Hamiltonian theory applied to hydrogen on nickel, J. Chem. Phys. 106 (1997) 8862.
[45] H. Nakatsuji, H. Nakai, Chem. Phys. Lett. 174 (1990) 283.
[46] H. Nakatsuji, H. Nakai, Can. J. Chem. 70 (1992) 404.
[47] H. Nakatsuji, H. Nakai, Chem. Phys. Lett. 197 (1992) 339.
[48] H. Nakatsuji, H. Nakai, J. Chem. Phys. 98 (1993) 2423.
[49] P.J. van der Hoek, A.W. Kleyn, E.J. Barends, Comments At. Mol. Phys. 23 (1989) 93.
[50] Q. Ge, P. Hu, D.A. King, M.H. Lee, J.A. White, M.C. Payne, J. Chem. Phys. 106 (1996) 1210.
[51] J.H. Lin, B.J. Garrison, J. Chem. Phys. 80 (1983) 2904.
[52] A. Eichler, J. Hafner, Molecular precursors in the dissociative adsorption of O_2 on Pt(111), Phys. Rev. Lett. 79 (1997) 4481.
[53] G. Ihm, M.W. Cole, F. Toigo, G. Scoles, J. Chem. Phys. 87 (1987) 3995.
[54] R. Kosloff, Time-dependent quantum-mechanical methods for molecular dynamics, J. Phys. Chem. 92 (1988) 2087.
[55] R. Kosloff, Propagation methods for quantum molecular dynamics, Annu. Rev. Phys. Chem. 45 (1994) 145.
[56] R. Kosloff, H. Tal-Ezer, A direct relaxation method for calculating eigenfunctions and eigenvalues of the Schrödinger equation on a grid, Chem. Phys. Lett. 127 (1986) 223.
[57] G. Katz, R. Kosloff, J. Chem. Phys. 103 (1995) 9475.
[58] I. Zoric, B. Kasemo, personal communication, 1998.